Ann. Geophys., 26, 77–86, 2008
www.ann-geophys.net/26/77/2008/

Annales Geophysicae

Parameterization of ionization rate by auroral electron precipitation in Jupiter

Y. Hiraki[1] **and C. Tao**[2]

[1]Graduate School of Energy Science, Kyoto University, Uji, Japan
[2]Department of Geophysics, Tohoku University, Sendai, Japan

Received: 12 April 2007 – Revised: 7 November 2007 – Accepted: 17 December 2007 – Published: 4 February 2008

Abstract. We simulate auroral electron precipitation into the Jovian atmosphere in which electron multi-directional scattering and energy degradation processes are treated exactly with a Monte Carlo technique. We make a parameterization of the calculated ionization rate of the neutral gas by electron impact in a similar way as used for the Earth's aurora. Our method allows the altitude distribution of the ionization rate to be obtained as a function of an arbitrary initial energy spectrum in the range of 1–200 keV. It also includes incident angle dependence and an arbitrary density distribution of molecular hydrogen. We show that there is little dependence of the estimated ionospheric conductance on atomic species such as H and He. We compare our results with those of recent studies with different electron transport schemes by adapting our parameterization to their atmospheric conditions. We discuss the intrinsic problem of their simplified assumption. The ionospheric conductance, which is important for Jupiter's magnetosphere-ionosphere coupling system, is estimated to vary by a factor depending on the electron energy spectrum based on recent observation and modeling. We discuss this difference through the relation with field-aligned current and electron spectrum.

Keywords. Ionosphere (Auroral ionosphere; Ionosphere-magnetosphere interactions; Particle precipitation)

1 Introduction

The stable and bright main auroral oval on Jupiter is almost corotating with the planet. The main oval is considered to be associated with the field-aligned current caused by the interaction between plasmas in the ionosphere and those in the magnetosphere (e.g. Hill, 1979, 2001). Assuming conservation of the angular momentum, nearly corotating plasmas lag behind the planetary rotation when they are transported outward from the Io torus. In the reference frame of the planetary rotation, a corotation electric field is induced in the ionosphere toward low latitude, and the Pedersen current flows along this field. The current flows out easily toward the magnetosphere along magnetic field lines, since the electric field becomes weak at low latitude due to nearly corotating plasmas in the inner magnetosphere. The upward field-aligned current is carried principally by downward precipitating electrons, which leads to the formation of the main oval. In the magnetospheric equator, the outward current enforces lagging plasmas by Ampère's force to corotate with the planetary rotation. In fact, observed angular velocity of the plasmas is higher than that without this torque transfer from the ionosphere. It is essential to know temporal and spatial distributions of the Pedersen conductance for understanding the characteristics of the corotating aurora and the interaction between magnetospheric and ionospheric plasmas (e.g. Nichols and Cowley, 2004). Their results show that both the magnitude and structure of the field-aligned current vary dramatically by considering the variation of the Pedersen conductance as a function of auroral flux, or current density. In general, the conductance varies with (1) atmospheric ionization and thermalization processes through collisions between auroral electrons and neutral particles, (2) Joule heating due to the convective electric field in the magnetosphere, and (3) atmospheric ionization and thermalization by solar EUV. Ionization by auroral electrons changes the plasma density, which directly affects the conductance, especially at the high latitude auroral region; thus it makes the largest contribution among these processes. We neglect the effect of other precipitating particles, such as proton, O^+, and S^{2+}, on the basis of observed auroral spectrum at the main oval region (Clarke et al., 1994; Waite et al., 1994; Liu et al., 1998).

Altitude distribution of the ionization rate by auroral electrons has been estimated with several methods, one of which is the continuous slow down approximation for the transport

Correspondence to: Y. Hiraki
(hiraki@center.iae.kyoto-u.ac.jp)

Published by Copernicus Publications on behalf of the European Geosciences Union.

of auroral electrons (Gerard and Singh, 1982; Rego et al., 1994; Prangé et al., 1995). Jovian Ionospheric Model (JIM) (e.g. Achilleos et al., 1998) uses a simplified one-downstream model, while the Jupiter Thermospheric General Circulation Model (JTGCM) (Bougher et al., 2005) refers to the calculated result of a two-stream model by Grodent et al. (2001). Evaluation of the effect of auroral electrons in each time step requires a great deal of time and decreases computational efficiency. Since ionization and heating rates depend on the temporally and spatially variable conditions of neutral atmosphere (i.e. temperature and density) and of auroral electrons (i.e. energy flux and incident angle distribution), adaptation of the results from other models would create a large error. The purpose of this study is to provide a simple and useful formula of the ionization rate by auroral electrons that will be applicable to the general circulation model and to the precise estimation of the variation in the ionospheric conductance.

Parameterization of the ionization rate by auroral electrons has been already provided for the case of the Earth by Rees (1963); the expression is shown in Sect. 3.1. We multiply the rate (/m) by the electron flux to obtain the ionization rate (/m^3/s), and then multiply further by the ionization potential and heating efficiency to estimate the heating rate of neutral gas (K/m^3/s). We calculate the penetration process of monochromatic electrons into Jupiter's H_2 atmosphere using a Monte Carlo method (Sect. 2). We perform the parameterization of ionization rate referring to the Rees formula and do its verification in Sect. 3, and finally discuss the estimated conductivity in Sect. 4.

2 Numerical simulation

2.1 Model description

We explain here details of the Monte Carlo method used to derive the ionization rate by auroral electrons. Sample M particles with incident energy ε_0 are initially positioned at the altitude $z_{\rm init}$, where their initial velocities as $(v_z, v_y)=(-\sqrt{2\varepsilon_0/m}, 0)$, m being the electron mass and y the lateral direction. We solve their equations of motion without any external forces, such as the electric field in the acceleration region; they are assumed to be already fully accelerated. The cyclotron motion of electrons is replaced by the simple bulk motion along the intrinsic magnetic field line. The calculation is over when the energies of all particles are reduced to $\approx$1 eV, which is low enough not to affect the results. We count the number of ionization collision $n_{\rm ion}(z)$ in each altitude through the calculation and obtain the ionization rate per unit length in height per one incident electron as $q_{\rm ion}=n_{\rm ion}/M/\Delta z$, the bin size Δz=10 km. We perform calculations in the energy range of ε_0=0.5–200 keV with the number M=5000–20 000. It is confirmed that the bin size Δz and the sample number M are enough not to affect the altitude dependence and magnitude of $q_{\rm ion}$. We set the altitude $z_{\rm init}$ in the range of 2500–3000 km. We can neglect the energy loss above this altitude through their precipitation; the H_2 density in this range is $\leq 10^7$ cm^{-3} and the collision cross section of H_2 and electron with 1 keV energy is $<10^{-16}$ cm^2, thus their mean free path is estimated to be $>10^4$ km.

We consider only H_2 as a collision partner of electrons because of its abundance in the target region. We adopt the Monte Carlo method based on the null collision technique (Vahedi and Surendra, 1995). The probability of a collision within the time Δt is given as $P_{\rm i}=1-\exp(-N(z_{\rm i})\sigma_{\rm tot}(\varepsilon_{\rm i})v_{\rm i}\Delta t)$, $N(z)$ the total atmospheric gas density at an altitude z, $\sigma_{\rm tot}$ the sum of the collision cross sections considered, while $z_{\rm i}$, $\varepsilon_{\rm i}$, and $v_{\rm i}$ being the position, energy, and velocity of i-th electron, respectively. A collision occurs if it obtains a random number $R\leq P_{\rm i}$, where $R\in[0,1]$. Our model allows only one collision per electron in Δt, so that the number of missed collisions should be lowered; the time step is set to be $\Delta t\approx 10^{-10}$–10^{-8} s to meet $P_{\rm i}<0.1$, with the probability of a multiple collision being less than 1%. For each of the collided electrons we decide the collision type using the cross sections and another random number. We consider ten collision types: elastic scattering, total ionization, including dissociative ionization, vibrational excitation (v=1), rotational excitation ($J=0\rightarrow 2$), and electronic excitations of B and C singlet states and a, b, c, e triplet states. These cross sections are taken from Tawara et al. (1990), all the peak values of which exceed 10^{-17} cm^2 (shown in Fig. 12). For elastic scattering, ionization, and excitations of B and C, dependence of the scattering angle on injected electron energy is given by the screened Rutherford formula (Lummerzheim et al., 1989), whereas it is isotropic for others. The former scattering angle distribution is dominated by forward scattering ($<10^\circ$) in the case of $\varepsilon_0>1$ keV, while approaches being isotropic for <100 eV case. For ionization, dependence of the energy partitioning between scattered and secondary electrons on the injected energy is given by Vahedi and Surendra (1995) as a smooth function. For example, a secondary electron becomes predominantly an energy of <50 eV, determined by a random number, through a collision of the 1 keV electron with H_2. We neglect both the momentum transfer between H_2 and electron through collision and the thermal velocity of the molecule. This assumption is valid because the neutral temperature is around 1000 K even when it goes up by auroral heating on the basis of calculation results of the JIM (Achilleos et al., 1998). The H_2 density we use for calculation is expressed as

$$N_{\rm H_2}(z) = 6.8\times10^{19}\exp(z'/62)+2.7\times10^{18}\exp(z'/180) + 6\times10^{16}\exp(z'/350),\ z'=300-z \quad (1)$$

in units of 1/m^3 with z in km, where the zero level corresponds to a pressure of 1 bar. This value is referred to Kim et al. (2001) to be estimated from observations of the Galileo spacecraft.

2.2 Results and validation

Figure 1 shows altitude distributions of the ionization rate $q_{\rm ion}$ calculated in the above conditions for the cases of initial electron energy ε_0=0.5, 1, 5, 10, 50, 100, and 200 keV. It is clearly seen that electrons with higher energy can precipitate into a deeper region, and the ionization rate itself becomes larger. For the respective cases of initial energy, the stopping altitudes $z_{\rm min}$ are 1260, 1040, 640, 530, 350, 280, and 220 km. The ionization rate becomes broad for the low energy cases whereas it has a sharp peak for the high energy cases. This tendency is due to the smallness of the scale-height of H_2 density at low altitude and is, furthermore, due to the time-integrated energy distribution of electrons at each altitude (discussed later). The peak values are almost proportional to ε_0.

We try to verify the applicability of our model to realistic conditions. We investigate the effects on $q_{\rm ion}(z)$ of (i) electron impact on helium, secondly abundant in the Jovian atmosphere, and of (ii) the uncertainty in the high-energy tails of the e-H_2 collision cross sections. For e-He collision the sum of electronic excitations, total ionization, and elastic scattering are considered, the respective cross sections being taken from Jackman et al. (1977), the database of the National Institute for Fusion Science (NIFS), and the database by A. V. Phelps (JILA); see Fig. 12. For excitation and ionization the respective energy losses of electrons are assumed to be 22 and 24.58 eV. The He density is set to be $N_{\rm He}$=$9.2\times10^{18}\exp(z'/62)$ (e.g. von Zahn et al., 1998); the H_2 density is fixed as Eq. (1), its mixing ratio increases with decreasing altitude and is up to ≈13% below 400 km. We perform test simulations in the cases of ε_0=50 keV and 100 keV, and show the results in Fig. 2a. With the energy loss by e-He collision being larger, the stopping heights become higher by including the process. Since the magnitude itself of the cross sections is the same as that of e-H_2 cross sections, the collision probability is roughly determined by the mixing ratio; thus, changes in $q_{\rm ion}$ are limited by less than 10%. We can consider that the ionization rate is mostly governed by the major component.

Next, we evaluate the effect on $q_{\rm ion}$ of uncertainty in the B and C excitation cross sections, especially at these high energy parts. Here, the H_2 density is fixed as Eq. (1), without inclusion of He. Tawara et al. (1990) showed reference values of cross sections in the energy range ≤1 keV; when we extrapolate these values with logarithmically straight lines the cross sections of B and C states exceed that of ionization around 30 keV due to a difference in these drops on energy. We make a test simulation in the case of ε_0=50 keV, where values for both excited states have the same drop as for ionization over 30 keV. This change brings about a decrease in the stopping height, as shown in Fig. 2b. Furthermore, the peak value of the ionization rate becomes large. We conclude that the change in cross sections affects slightly the characteristics of the mean energy loss and scattering that electrons experience through their precipitation. This effect will appear in the height-integrated conductivity (conductance), which is the key parameter for the magnetosphere-ionosphere coupling system of our interest. However, we only point out the existence of a potential error in our calculation and suggest future assessments on this subject.

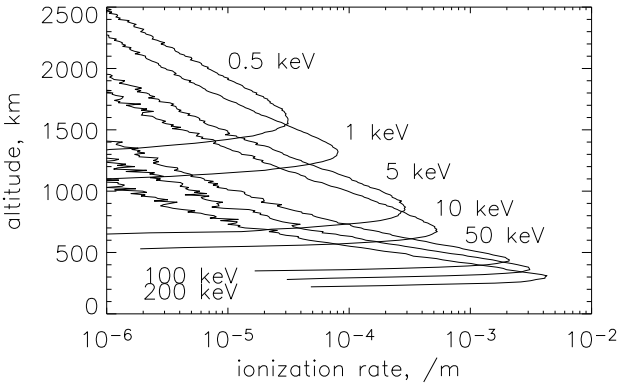

Fig. 1. Altitude distribution of ionization rate $q_{\rm ion}$ per electron with initial energy ε_0=0.5, 1, 5, 10, 50, 100, and 200 keV.

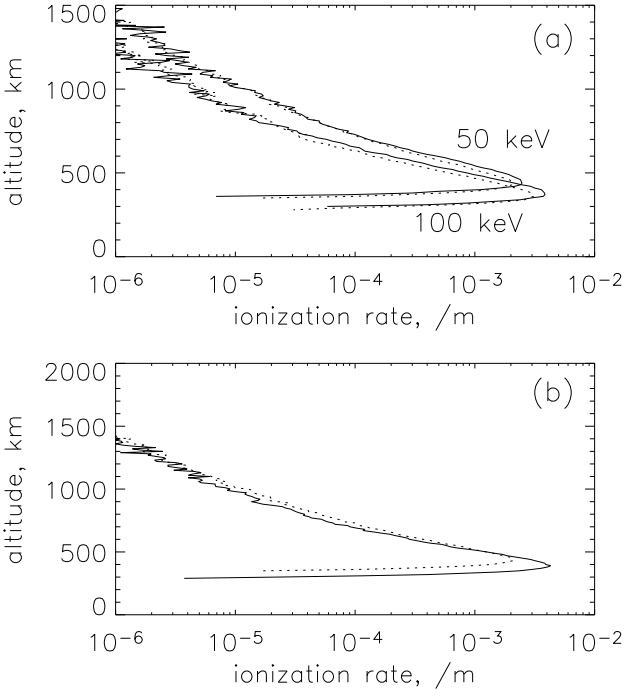

Fig. 2. (a) Effect of electron-helium collision on the total ionization rate for the cases of ε_0=50 and 100 keV. The solid and dotted curves are calculated with and without including He, respectively (see text for the detail of He parameters). **(b)** Effect of uncertainty in electron-hydrogen electronic excitation cross sections for the case of ε_0=50 keV. Dotted line is the original one, while the solid line is the result modified (see text).

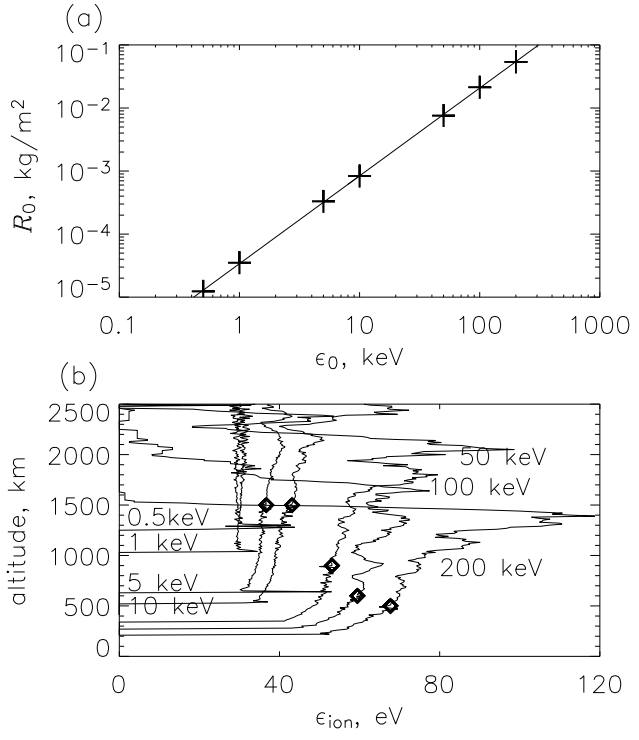

Fig. 3. (a) The column mass density R_0 of air above the stopping height of electrons as a function of their initial energy ε_0. The solid line shows a fitted function of $3.39\times10^{-5}\varepsilon_0^{1.39}$. **(b)** Altitude distribution of the average ion-yield energy $\varepsilon_{\rm ion}$, above the altitude denoted by diamonds, which are smoothed between 10 points for the sake of the exclusion of a large noise.

3 Parameterization of ionization rate

3.1 Parameterization

We apply the following formula by Rees (1963) to represent the calculation results of $q_{\rm ion}$ (/m) shown in Fig. 1,

$$q_{\rm ion}(\varepsilon_0, z) = \frac{\varepsilon_0}{\varepsilon_{\rm ion}} \frac{\lambda(z)}{R_0(\varepsilon_0)} \rho(z), \quad (2)$$

where $\varepsilon_{\rm ion}$ is the ion/electron pair yield energy ($\approx$35 eV for Earth's atmosphere), λ is a non-dimensional parameter representing the altitude distribution. The mass density ρ (kg/m^3) of neutral gas in our case is equal to $m_{\rm H_2} N_{\rm H_2}$, $m_{\rm H_2}=3.32\times10^{-27}$ kg and $N_{\rm H_2}$ is given as Eq. (1). The column mass density R_0 (kg/m^2) is defined as the integration of ρ above the stopping height $z_{\rm min}(\varepsilon_0)$ and is shown in Fig. 3a. Calculated values of R_0 have a clear positive correlation, which is well fitted by $R_0=3.39\times10^{-5}\varepsilon_0^{1.39}$ with ε_0 in keV. The ion yield energy $\varepsilon_{\rm ion}$ is derived as the ratio of total energy loss by all inelastic collisions to that by ionization at each altitude bin through the calculation. Figure 3b shows the dependences of $\varepsilon_{\rm ion}$ on altitude and ε_0; we would emphasize that inclusion of the altitude dependence is our new point from the formulation by Rees (1963) (Eq. 2)

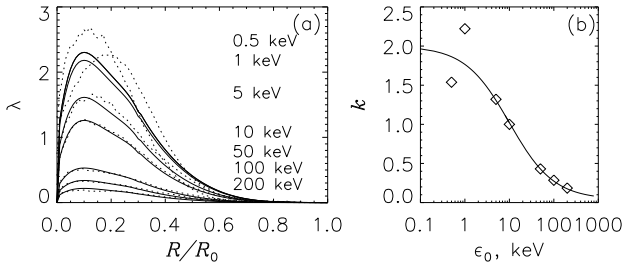

Fig. 4. (a) The profile function λ of the ionization rate as a function of the reduced column mass density R/R_0. The dotted curves show the calculated values with Eq. (2) directly by using $q_{\rm ion}$, R_0, and $\varepsilon_{\rm ion}$ in Figs. 1 and 3, whereas the solid ones are the scaled values of a fitted ε_0=10 keV one by using the ratio k (see text for the details of k). **(b)** The k values (diamonds) and fitted curve of the ε_0 dependence.

due to a rather exact multi-stream treatment. Noisy variation in $\varepsilon_{\rm ion}$ at high altitude, due to the smallness of the number of collisions, is removed by smoothing. For the case of $\varepsilon_0\leq$1 keV, $\varepsilon_{\rm ion}$ is almost constant as $\approx$30 eV without height dependence. The energy distribution of electrons at a certain altitude is mainly composed of an incident high-energy part and a secondary low-energy part produced by ionization. The height independence of $\varepsilon_{\rm ion}$ would be caused by constant consumption of the incident energy through collisional scattering. On the other hand, $\varepsilon_{\rm ion}$ increases and is up to 100 eV for the case of ε_0=200 keV. For the case of $\varepsilon_0\geq$10 keV, high-energy electrons penetrate without considerable scattering on their way and consume most of their energy around the stopping height, so that the ionization efficiency (the inverse of $\varepsilon_{\rm ion}$) has its maximum there. A decrease in the ionization efficiency at high altitude is due to a relatively small energy deposition as below the maximum of ionization cross section ($\approx$100 eV). An increasing trend in $\varepsilon_{\rm ion}$ with increase in ε_0 would be due to the predominance of excitation cross sections of B and C over the ionization cross section above 10 keV (note that it has an uncertainty, as discussed in the previous section). As to the simplicity and efficiency of the parameterization, we artificially divide the energy loss function as $\varepsilon_{\rm ion}=30\bar{\varepsilon}(\varepsilon_0, z)$ eV and redefine $\varepsilon_{\rm ion}$=30 eV and the new $\lambda(\varepsilon_0, z)$ as the old one divided by $\bar{\varepsilon}$. The ionization rate does not lose generality and accuracy through this operation.

Next, the parameter λ is derived by substituting $q_{\rm ion}$, R_0, and $\varepsilon_{\rm ion}$ into Eq. (2) and is shown in Fig. 4a as a function of R/R_0 and ε_0, where $R(z)$ is defined as an integral of ρ above a corresponding altitude z, $\lambda(R/R_0\geq1)=0$ and $R_0\equiv R(z_{\rm min})$. For simplicity, we divide λ into the energy-dependent variable $k(\varepsilon_0)$ and the height-dependent variable $\lambda_0(R/R_0)$. The λ_0 is selected as the value of the ε_0=10 keV case and is expressed as a function of $x=R/R_0$ as follows (Fig. 4a),

$$\lambda_0(x)=\begin{cases} -669.53x^4+536.18x^3-159.86x^2+18.586x+0.5064 & 0\leq x\leq0.3 \\ 0.767x^4-5.9034x^3+12.119x^2-9.734x+2.7470 & 0.3\leq x\leq0.825 \\ -0.8091x^3+2.4516x^2-2.4777x+0.8353 & 0.825\leq x\leq1. \end{cases} \quad (3)$$

Note that (for users) x should be defined for each ε_0 since it is an implicit function of ε_0 through R_0, although the profile itself of $\lambda_0(x)$ is independent of ε_0. The peak altitude of $q_{\rm ion}$ corresponds to $x_{\rm peak} \approx 0.29$, independent of ε_0, and the form of k is defined as $k(\varepsilon_0)=\lambda(\varepsilon_0, x_{\rm peak})/\lambda(10\,{\rm keV}, x_{\rm peak})$, shown in Fig. 4b. It has a negative correlation with ε_0, as clearly seen in Fig. 4a. This is because the increasing rate in $\rho(z_{\rm peak})$ with ε_0 is larger than that in $q_{\rm ion}$ in Eq. (2). Qualitatively, it may result from a rapid decrease in the scale height at lower altitude. The k is fitted smoothly by the following equation,

$$k(\varepsilon_0) = 0.13 + 0.89(1 - 1.1\tanh(\log_{10}\varepsilon_0 - 1)) \quad (4)$$

with ε_0 in keV. We can obtain $\lambda(\varepsilon_0, R/R_0)=k(\varepsilon_0)\lambda_0(R/R_0)$ for an arbitrary ε_0 using Eqs. (3) and (4), as shown in Fig. 4a. A noticeable shift in the peak position of λ for ε_0=1 keV may be due to several complicated factors. In addition, the absolute values of λ parameterized for the ε_0=0.5 and 1 keV cases have large deviations from the calculated ones. However, these deviations have little effect on the ionization rate and the conductance of our interest for the case of a plausible auroral energy spectrum. This is because the average energy of the spectrum is much higher, as several tens keV (discussed in the next section) and because the conductance is hardly sensitive to the deviations, as shown in Fig. 10a. Finally, we obtain the formula of the ionization rate using λ, as well as the preceding R_0 and $\varepsilon_{\rm ion}$=30 eV,

$$q_{\rm ion}(\varepsilon_0, z) = \frac{\varepsilon_0}{\varepsilon_{\rm ion}} \frac{\lambda(\varepsilon_0, R/R_0(z))}{R_0(\varepsilon_0)} \rho(z). \quad (5)$$

The results obtained from this parameterization are shown in Fig. 5 and agree well with the calculated profiles for the $\varepsilon_0 \geq 5$ keV cases. We could not find a reason for the differences in the profiles for the 0.5 and 1 keV cases, also shown as the differences in λ in Fig. 4; note again, that these do not affect the estimation of the conductance. We can construct the ionization rate $q_{\rm ion}(\varepsilon_0, z)$ by electron precipitation with an arbitrary energy in an arbitrary distribution of the H_2 atmosphere. The ionization rate for an arbitrary energy spectrum can be provided by integrating $q_{\rm ion}(\varepsilon_0, z)$ multiplied by the electron flux function $F(\varepsilon_0)$ over ε_0.

We define θ as the angle between the averaged velocity vector of electrons and the local vertical; in the previous section we set it as θ=0. With the angle being nonzero in actual case, it would be crucial to the ionization rate since the scattering processes include anisotropy. We make a further calculation by varying θ and its parameterization. The H_2 density is given by the same form as Eq. (1), and the initial velocity of electrons is expressed as $(v_z, v_y)=(-v_0\cos\theta, v_0\sin\theta)$. The θ dependence of $q_{\rm ion}(z)$ in the case of ε_0=10 keV is shown in Fig. 6b. In the range of $\theta \leq 30$ deg no remarkable difference from the case of θ=0 is seen in the altitude distribution. As to over 60 deg it is clearly seen that the ionization rate above 1200 km increases,

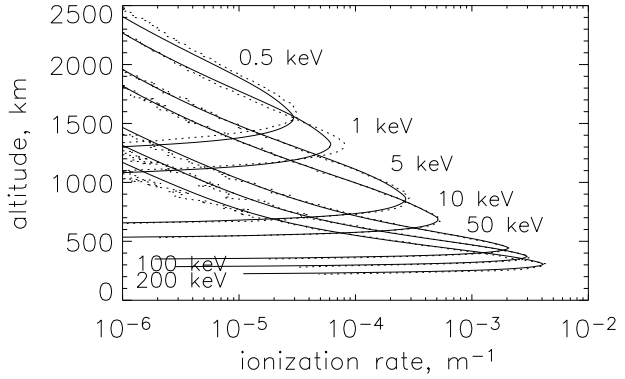

Fig. 5. Shown are parameterized $q_{\rm ion}$ values (solid), and are compared with the calculated ones (dotted) in Fig. 1.

while that below decreases, with an increase in θ. This is because for the case of the larger angle collision occurs more frequently at high altitude due to an extension of the flight distance of electrons, whereas the amount of energy dissipated at low altitude becomes smaller. It is remarkable that the stopping height is almost independent of the angle θ. This is because the height is controlled by secondary electrons. From these facts and the temporal variation of the ionization rate (not shown) we can diagnose the dynamics of high-energy electrons from their injection into atmosphere to their extinction. They penetrate easily to the peak altitude of $q_{\rm ion}$ with a slight energy loss, and lose the remnant energy around there. We can suppose that the peak altitude and the magnitude of ionization rate are controlled by the initial conditions ε_0 and θ, respectively, if the atmospheric conditions are identical. The secondary electrons produced around there are scattered isotropically and expand a little the scale they occupy. Therefore, the initial information on θ is already lost in the formation of a stopping height. The above statements agree perfectly with the discussion made when we introduce $\varepsilon_{\rm ion}$. We would describe our parameterization based on the results in Fig. 6. As for the previous one we derive $\lambda(\theta, x)$ and take $\eta(\theta, x)=\lambda(\theta, x)/\lambda(0, x)$, $\lambda(0, x)$ being defined by Eqs. (3) and (4). The values are shown in Fig. 6a and are expressed as the following equations:

$$\eta(\theta, x)=\begin{cases} 1 & 0<x\leq 10^{-c_0} \\ -a(\log_{10}x+c_0)(\log_{10}x+c)+1 & 10^{-c_0}<x\leq 10^{-c} \\ (10^{-c}/x)^b & 10^{-c}<x\leq 1 \\ 0 & 1<x, \end{cases} \quad (6)$$

$$a = \frac{\frac{0.5}{\cos\theta} + 0.5 - 1}{\frac{(c_0+c)^2}{4} - c_0 c},$$

$$b = -\frac{\log_{10}(0.75\cos\theta + 0.25)}{c - 0.523},$$

$$c = -\log_{10}(-0.0436\theta^2 + 0.0499\theta + 0.0302).$$

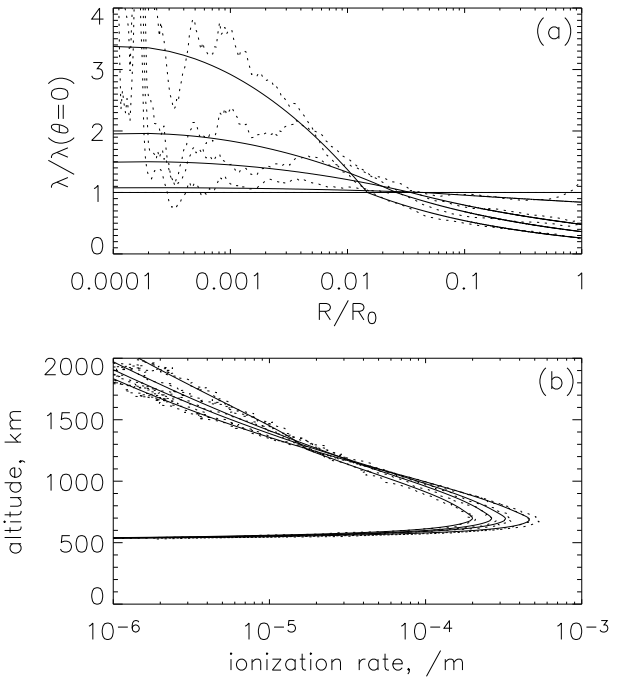

Fig. 6. Dependences of **(a)** parameter λ and **(b)** ionization rate on the tilt angle θ from the vertical line of initial electron velocity for the cases of ε_0=10 keV and θ=30, 60, 70, and 80 degrees (dotted: calculated, solid: parameterized by Eq. 6). For (a) the ratios to the one of θ=0 in Fig. 4 are shown. For (a) the deviation at $R/R_0<0.01$ increases and for (b) the magnitude at higher altitude increases (the peak decreases) with increasing θ, respectively.

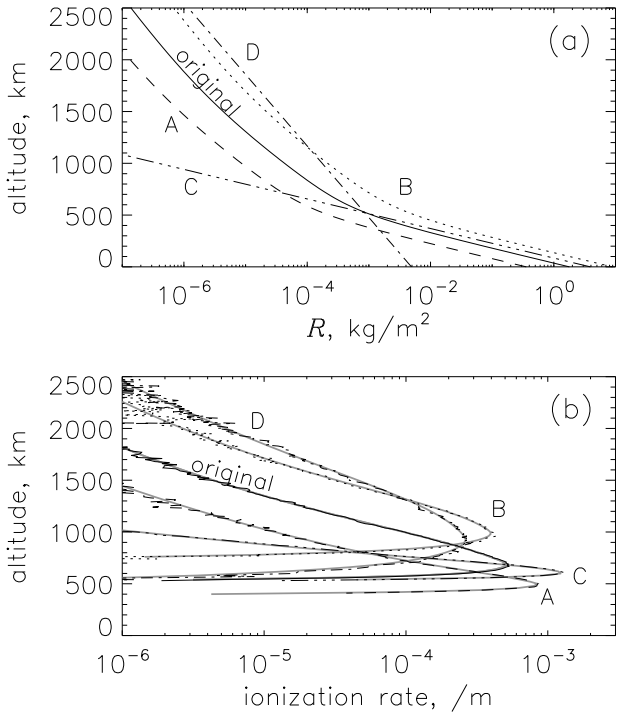

Fig. 7. Examples of the application of our parameterization to various cases of the H_2 density distribution **(a)**; in **(b)** the solid and dotted lines show the results from parameterization and from calculation, respectively.

As a result we obtain the ionization rate for an arbitrary flux $F(\varepsilon_0, \theta)$, multiplying $q_{\rm ion}$ in Eq. (5) by this η. Here the unit of θ is radian, $x=R/R_0$, and c_0=6.

3.2 Comparison with previous studies

It is not obvious that our parameterization is applicable to any distribution of the H_2 density other than the form of Eq. (1). Here we make a test with several forms of N_{H_2} for validation. The results of direct calculations using the Monte Carlo method and those from parameterization are shown in Fig. 7. The initial energy of electrons is set to be ε_0=10 keV. The two forms are 1/5 and 5 times the magnitude of Eq. (1), shown with respective lines A and B. For the other two, the scale-height is changed to be steeper or slower than that in Eq. (1), with the electron stopping height unchanged; the explicit forms are $N_{H_2}=1.5\times10^{20}\exp(z'/62)$ and $1.8\times10^{18}\exp(z'/300)$, shown with respective lines C and D. Success of our parameterization is clearly seen in Fig. 7b. The similar results are expected for other energy cases, although the fitting error becomes large for low energy cases ($\leq$1 keV).

Next, we would compare our result with that obtained by Grodent et al. (2001) with a two-stream approximation of the Boltzmann equation. They show the ion production rate $\int q_{\rm ion}(z, \varepsilon_0)F(\varepsilon_0)\mathrm{d}\varepsilon_0$ with units of /m^3/s when the electron energy flux at the top of the atmosphere is represented as a tri-Maxwellian distribution function to create discrete aurora; the profile is shown in Fig. 8a. We calculate the ionization rate using our parameterization under the same conditions of the electron flux and the H_2 density, not equal to Eq. (1), and derive the ion production rate as also shown in Fig. 8a. It is found that our result agrees well with that of Grodent et al. (2001) from the peak to 1000 km and over 1300 km. However, the difference in the sub-peak around 1200 km is up to the factor of 4. This peak is produced by the lowest energy component (100 eV) of the triplet distributions. It is checked that the difference is not due to the error in parameterization discussed regarding λ for $\varepsilon_0\approx$1 keV, although this energy range has the largest contribution to the sub-peak. It is also checked that the difference is much larger than the systematic error when we read their data. It may not be due to the effect of atomic hydrogen H because its contribution to the total ionization rate is quite small, by 1–2 orders in their calculation. The possible factors are the differences in numerical scheme and cross section data. We do not mention more details of the difference, by the order of 2 smaller than the peak value, judging from the negligible contribution to the estimation of the conductance.

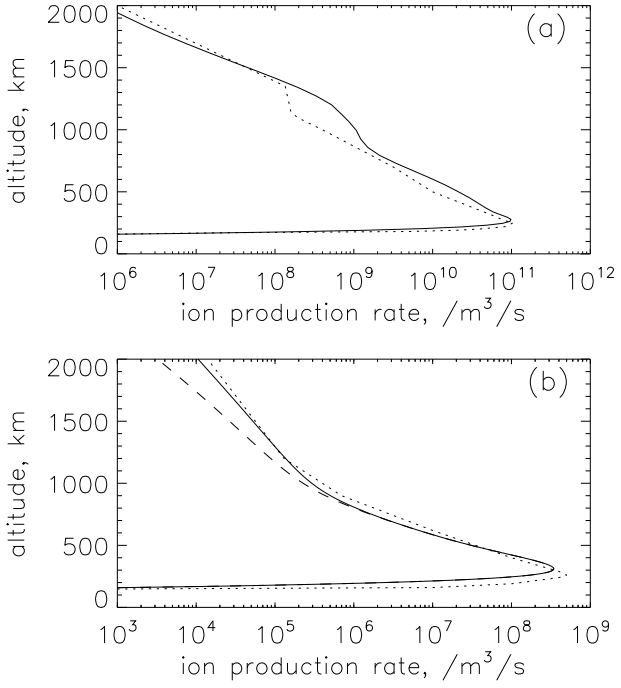

Fig. 8. (a) Comparison of an ion production rate $q_{\rm ion}F$ by our parameterization (solid) with the previously presented value by Grodent et al. (2001) (dotted), F the electron flux. **(b)** Comparison of our parameterized ionization rates with that (dotted line) by Rego et al. (1994). Solid (dashed) line represents the rate produced based on the H+H_2 (pure H_2) density distribution and electron energy spectrum they adopted (see text for details).

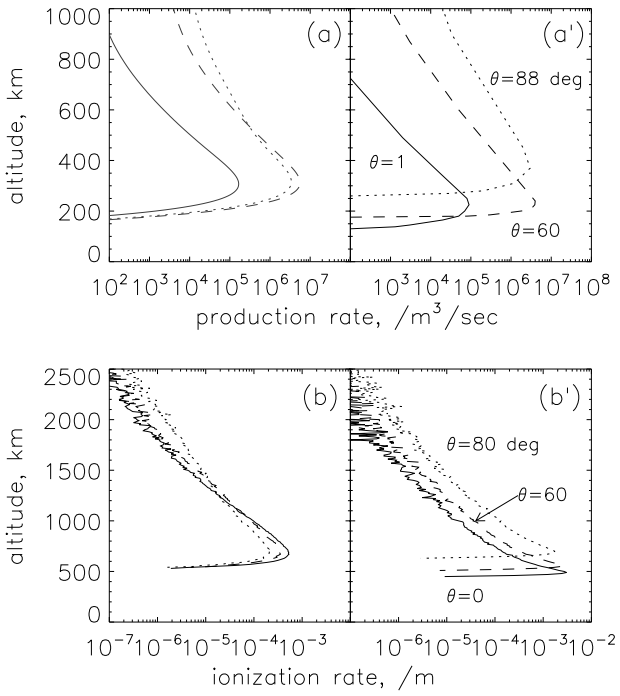

Fig. 9. Comparison of our ionization rates **(a)** with the excitation rate **(a')** by Prangé et al. (1995); in both the incident angles of electrons are 1 (solid-line), 60 (dashed), and 88 (dotted) degrees, and the energy flux is 1 erg/cm^2/s/(2π sr). **(b')** shows test results where the moving direction of both the primary and secondary electrons is fixed as θ all through the calculation; **(b)** shows our results with no assumption; these line types are for the same incident angles as those in (b').

We compare our results further with those by Rego et al. (1994). They calculated ionization rates with the slowdown method for electrons (Gerard and Singh, 1982). We also examine the effect of atomic hydrogen H, abundant in high altitude >1000 km, that they included. In this examination we assume simply the ionization rate for e-H collision as one half of $q_{\rm ion,H_2}$ since the cross section for e-H collision has similar properties to the e-H_2 one, except that the peak value of the former is almost half that of the latter; Rego et al. (1994) used a similar assumption. Figure 8b shows by a solid line the ion production rate using the parameterization in the similar conditions to their case: the electron energy spectrum as a Maxwellian distribution with a peak at 10 keV, and the same atmospheric density profile. The rate at high altitude increases by the factor of 2–3 while the rate at the peak is almost unchanged compared to that without H. On the basis of negligible importance of this difference at high altitude (with smaller magnitude of 10^3 than the peak value) on the estimation of conductance, we conclude that the influence of H would be small and do not include it in our parameterization. We find that the rate including H is quite consistent with that of Rego et al. (1994) (dotted-line), except for the peak and stopping altitudes. The inconsistency would be caused by the difference in calculation methods and will be mentioned in the next paragraph.

Finally, we compare our results of the electron incident-angle dependence with the similar study by Prangé et al. (1995), who applied the same method by Rego et al. (1994). Their results in Fig. 9a' show the excitation rates of the H_2 Lyman band (B-state excitation) by monochromatic electrons with several incident angles. As a comparison we also show the obtained ionization rates in the same condition (Fig. 9a). We regard that the ionization rates are comparable with the excitation rates, since both the energy range and magnitude of these two cross sections are quite similar; the figures show actually the peak values agree well within an expected difference by dozens of percent. The peculiar dependence of the peak values on θ is due to the normalization of the angular distribution of primary electrons weighted by $\sin\theta {\rm d}\theta$. We would mention the critical difference in the θ dependence of the peak and stopping altitudes, i.e. their results vary widely by several hundreds, while ours do not. We take notice of the treatment of moving direction of the electrons. Prangé et al. (1995) fixed the direction as θ all through the calculation, as Rego et al. (1994) did, while we

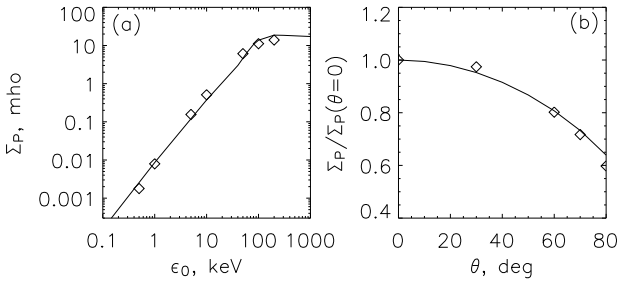

Fig. 10. Dependences of the height-integrated Pedersen conductivity on initial **(a)** energy ε_0 and **(b)** tilt angle θ of electrons. Diamonds are obtained with Monte Carlo calculation results, while the solid lines are from parameterization (details in text).

treat it variable in each electron through collision. In order to elucidate this effect we perform calculations with the similar restriction that the moving direction of both primary and secondary electrons is fixed as θ (Fig. 9b'). We can find that both peak and stopping altitudes vary remarkably, depending on the incident angle compared to the original ones (Fig. 9b, previously shown in Fig. 6b). As for the peak altitude, the energy loss of electrons through their precipitation may be underestimated due to the restriction of "fixed θ"; in fact, the angular distribution changes largely from the initial one through considerable scattering. The difference between Rego et al. (1994) and ours is also explainable by this effect. Our treatment would be more valid and new in this viewpoint. As to the stopping height, we find that its variation is due to an extension of atmospheric depth by $\sec\theta$ with the incident angle being fixed. We checked that the values of R_0 as a function of $N\sec\theta$ in all three cases in Fig. 9b' are in perfect accord. On the basis of the above comparison, we emphasize that our Monte Carlo method brings a major modification of estimation of not only the ionization rate itself but the conductance.

4 Discussion on conductance

We estimate the dependences of the Pedersen conductance on initial conditions ε_0 and θ of auroral electrons. The flux $F(\varepsilon_0)$ is fixed as 6.25×10^{12} /m^2/s for all cases. Assuming that the H_2^+ ions produced through the electron impact ionization of H_2 are being converted instantly to H_3^+, the local ion density n is given by the balance between this H_3^+ ion production and its loss through recombination with the electron. The collision frequencies ν of H_3^+ and electrons with H_2 are taken from Chapman and Cowling (1970) and Danby et al. (1996), respectively. Note that the Pedersen conductance used in this paper is not the effective one modified by the slippage of the neutral atmosphere from strict rigid corotation (Nichols and Cowley, 2004) but the original one simply defined as follows. Parallel conductivity σ being defined by n and ν, we derive the Pedersen conductivity $\nu^2\sigma/(\nu^2+\Omega^2)$, Ω the cyclotron frequency, the intrinsic magnetic field being assumed as 8.4 G, and obtain the conductance Σ_P by integrating it over the altitude range of 0–3500 km. Here we adopt the neutral density as Eq. (1) and the neutral temperature as that assumed in the JIM. The ε_0 and θ dependences of Σ_P are shown in Fig. 10a and b, respectively. A positive correlation of Σ_P with ε_0 is obvious since the ionization at low altitude contributes effectively. At the energy range <60 keV our values estimated in a simple manner agree well with the results by Millward et al. (2002) using the data of JIM. It is expected that the increasing rate in this range is quite similar to that of $R(\varepsilon_0)$, however, in fact, it is slightly steeper ($\propto \varepsilon_0^{1.65}$). This is because R corresponds to an integral of N only, while Σ_P is an integral of N convoluted by the ion density ($\propto\sqrt{N}$). It is seen that the increment in Σ_P is saturated at 80–100 keV, since the peak altitude of the ionization rate, equally of ion density, becomes lower than the peak of the ion mobility (≈400 km). The applicable energy limit seems to be around 300 keV, over which the model equations and the low-altitude atmospheric conditions are invalid. We find in Fig. 10b that Σ_P decreases with an increase in θ and the rate is up to 40%. This dependence corresponds to a reduction in the peak values of the ionization rate, as shown in Fig. 6b. It is considered to be up to 60%, if we estimate it by only the peak value; this overestimation may be due to the predominance of a contribution at lower altitude of 600 km where the ion mobility is higher.

Finally, we discuss the relation between ionospheric conductance Σ_P, field-aligned current $j_\parallel$, and electron energy spectrum at the main oval by referring to the simulation results by Nichols and Cowley (2004), in which the field-aligned current is treated self-consistently. The static relation between Σ_P and $j_\parallel$ should be the key of their model system. The number flux of the precipitating electrons from the magnetosphere, i.e. the current, is modulated immediately through changes in the conductance, which is the generator of the system. The acceleration rate of electrons in a parallel electric field at the top of atmosphere may be limited in reality, so that the increasing rate of the conductance is limited likewise. Suppose that this upper limit is controlled by the quasi-steady condition of ionosphere; one of the candidates is the peak altitude of ion mobility (≈400 km). Suppose further that the convergence of the Pedersen current at this altitude generates the field-aligned current associated with the main oval. Figure 5 shows that the electron with energy ε_0≈100 keV gives the peak of the ionization rate at this altitude. For a maximum estimation of conductance we prepare the energy flux function with its peak around the energy on the basis of the formulation in Nichols and Cowley (2004) and calculate $j_\parallel$ and Σ_P in a similar way as in the previous paragraph (Fig. 11a, b). Furthermore, we adopt two flux functions derived on the basis of observation results (Grodent et al., 2001; Gustin et al., 2004), with a simple normalization of these magnitudes to adjust $j_\parallel$. Variations in

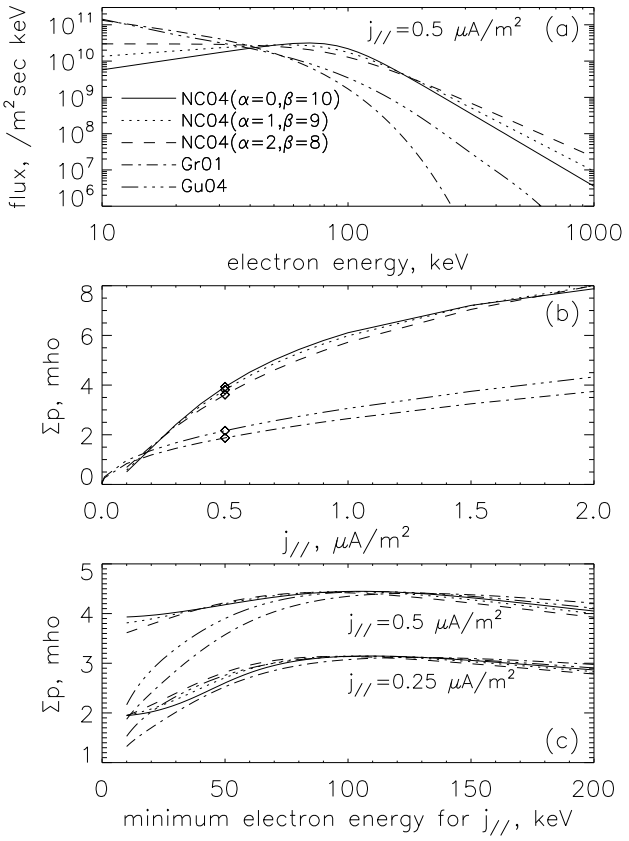

Fig. 11. (a) Assumed electron energy spectra with the current being fixed as $j_{\parallel}$=0.5 μA/m^2. NC04, Gr01, and Gu04 refer to those in Nichols and Cowley (2004), Grodent et al. (2001), and Gustin et al. (2004), respectively; α and β are control parameters of the slope of spectrum. **(b)** Pedersen conductance as a function of field-aligned current density obtained with each spectrum shown in (a). **(c)** Modified Pedersen conductance versus the base of integral energy range when the current is defined. The upper and lower 5-line sets correspond to $j_{\parallel}$=0.5 and 0.25 μA/m^2 cases, respectively. Line types used are identical in all figures.

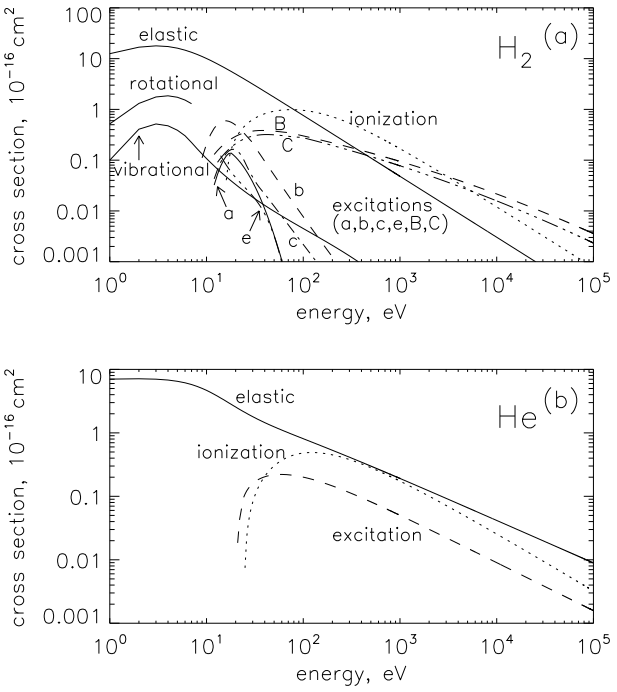

Fig. 12. Electron impact cross sections of **(a)** H_2 and **(b)** He for various collision processes.

the conductance through spectral configurations are shown in Fig. 11b. For comparison we choose the current density as $j_{\parallel}$=0.5 μA/m^2 derived from the former cases of a spectral peak around 100 keV. It is shown that the conductance at this current is $\Sigma_P \approx 4$ mho with small variation on the spectra, whereas the conductance in the other two cases is smaller by a factor of 2. This may be due to the effect of the low energy component of spectra in Grodent et al. (2001) and Gustin et al. (2004) to reproduce observed high atmospheric temperature. Assuming that the low energy component cannot reach the peak altitude of ion mobility, we try to eliminate the component from the definition of current $j_{\parallel}$. Figure 11c shows that the variation in conductance ($\approx$100% seen in Fig. 11b) is reduced down to several tens of percent, with an increase in the base of the energy integral as over 15 keV. The conductance and current in the above estimation are larger than the calculated results in Nichols and Cowley (2004), $j_{\parallel}$=0.25 μA/m^2 and Σ_P=1.5 mho, which is consistent with recent observation. The differences in these values from ours may be related with the fact that the peak electron energy in their spectrum is slightly lower than that to reach the peak altitude of ion mobility. However, the effects of the actual tilt angle of the magnetic field line and the finite pitch angle would reduce our values of conductance and current to a certain extent. We consider that the variation in Σ_P (the factor of two) is under the resolution of observation at present. We hope, at least, the direct particle observation used to obtain the ratio of a low (10–20 keV) to high (80–120 keV) energy component of electron flux, and the magnetic field observation used to obtain the field-aligned current around the 400-km altitude with resolution of 0.1 μA/m^2, both lead to a detailed understanding of the source of the field-aligned current at the main oval region.

5 Summary

We simulate the penetrating process of auroral electrons into Jupiter's H_2 atmosphere with a Monte Carlo method and present a simple parameterization of the ionization rate, referring to the formula used in previous studies on the Earth. We confirm that the conductance, the key parameter for the magnetosphere-ionosphere coupling system, estimated with the parameterized ionization rates agrees with the exact one

by numerical simulation, as well as that estimated by the previous study within systematic errors. We also confirm that the ionization rate in any distribution of atmospheric density is highly reproducible, so that it can be applied to the case of the other outer planets with a major component of H_2. To verify our model and parameterization we examine that the influences of He and H are negligible, less than 10%, on the ionization rate, whereas uncertainty in the high-energy part of the electron-H_2 collision cross sections induces uncertainty by several factors. We further formulate the dependence on the incident angle of primary electrons and compare the results with previous studies using other approaches; we indicate the intrinsic problem of their approximation. Finally, we estimate the maximum values of the ionospheric conductance and the field-aligned current at the main oval region, assuming the electron energy spectrum on the basis of previous observation and modeling, and the ionospheric steady condition, such as for ion mobility; these show a variation by a factor of 2 and are 1–2 times larger than the simulation results by Nichols and Cowley (2004).

Acknowledgements. We take total ionization and elastic scattering cross sections of helium by electron collision from the atomic and molecular databases (ADMIS) of the National Institute for Fusion Science (NIFS) and the collision data compilation by A. V. Phelps at JILA respectively.

Topical Editor M. Pinnock thanks D. Lummerzheim and another anonymous referee for their help in evaluating this paper.

References

Achilleos, N., Miller, S., Tennyson, J., Aylward, A. D., Mueller-Wodarg, I., and Rees, D.: JIM: A time-dependent, three-dimensional model of Jupiter's thermosphere and ionosphere, J. Geophys. Res., 103(E9), 20 089–20 112, 1998.

Bougher, S. W., Waite Jr., J. H., Majeed, T., and Gladstone, G. R.: Jupiter Thermospheric General Circulation Model (JTGCM): Global structure and dynamics driven by auroral and Joule heating, J. Geophys. Res., 110, E04008, doi:10.1029/2003JE002230, 2005.

Chapman, S. and Cowling, T. G.: The Mathematical Theory of Non-Uniform Gases, Cambridge University Press, Cambridge, UK, 1970.

Clarke, J. T., Ben Jaffel, L., Vidal-Madjar, A., Gladstone, G. R., Waite Jr., J. H., Prangé, R., Gérard, J.-C., Ajello, J., and James, G.: Hubble Space Telescope Goddard High-Resolution Spectrograph H_2 rotational spectra of Jupiter's aurora, Astrophys. J., 430, L73–L76, 1994.

Danby, G., Elza, B. K., Morrison, M. A., and Trail, W. K.: The separable representation of exchange in electron-molecule scattering: I. Elastic scattering and rotational excitation, J. Phys. B: At. Mol. Opt. Phys., 29, 2265–2287, 1996.

Gérard, J.-C. and Singh, V.: A model of energy deposition of energetic electrons and EUV emission in the Jovian and Saturnian atmospheres and implications, J. Geophys. Res., 87(A6), 4525–4532, 1982.

Grodent, D., Waite Jr., J. H., and Gérard, J.-C.: A self-consistent model of the Jovian auroral thermal structure, J. Geophys. Res., 106(A7), 12 933–12 952, 2001.

Gustin, J., Feldman, P. D., Gérard, J.-C., Grodent, D., Vidal-Madjar, A., Ben Jaffel, L., Desert, J.-M., Moos, H. W., Sahnow, D. J., Weaver, H. A., Wolven, B. C., Ajello, J. M., Waite, J. H., Roueff, E., and Abgrall, H.: Jovian auroral spectroscopy with FUSE: analysis of self-absorption and implications for electron precipitation, Icarus, 171, 336–355, 2004.

Hill, T. W.: Inertial limit on corotation, J. Geophys. Res., 84(A11), 6554–6558, 1979.

Hill, T. W.: The Jovian auroral oval, J. Geophys. Res., 106(A5), 8101–8108, 2001.

Jackman, C. H., Garvey, R. H., and Green, A. E. S.: Electron impact on atmospheric gases I. Updated cross sections, J. Geophys. Res., 82, 5081–5090, 1977.

Kim, Y. H., Dean Pesnell, W., Grebowsky, J. M., and Fox, J. L.: Meteoric ions in the ionosphere of Jupiter, Icarus, 150, 261–278, 2001.

Liu, X., Shemansky, D. E., Ahmed, S. M., James, G. K., and Ajello, J. M.: Electron-impact excitation and emission cross sections of the H_2 Lyman and Werner systems, J. Geophys. Res., 103(A11), 26 739–26 758, 1998.

Lummerzheim, D., Rees, M. H., and Anderson, H. R.: Angular dependent transport of auroral electrons in the upper atmosphere, Planet. Space Sci., 37, 109–129, 1989.

Millward, G., Miller, S., Stallard, T., Aylward, A. D., and Achilleos, N.: On the dynamics of the Jovian ionosphere and thermosphere: III. The modelling of auroral conductivity, Icarus, 160, 95–107, 2002.

Nichols, J. D. and Cowley, S. W. H.: Magnetosphere-ionosphere coupling currents in Jupiter's middle magnetosphere: Effect of precipitation-induced enhancement of the ionospheric Pedersen conductivity, Ann. Geophys., 22, 1799–1827, 2004.

Prangé, R., Rego, D., and Gérard, J.-C.: Auroral Lyman α and H_2 bands from the giant planets: 2. Effect of the anisotropy of the precipitating particles on the interpretation of the "color ratio", J. Geophys. Res., 100(E4), 7513–7522, 1995.

Rees, M. H.: Auroral ionization and excitation by incident energetic electrons, Planet. Space Sci. 11, 1209–1218, 1963.

Rego, D., Prangé, R., and Gérard, J.-C.: Auroral Lyman α and H_2 bands from the giant planets: 1. Excitation by proton precipitation in the Jovian atmosphere, J. Geophys. Res., 99(E8), 17 075–17 094, 1994.

Tawara, H., Itikawa, Y., Nishimura, H., and Yoshino, M.: Cross sections and related data for electron collisions with hydrogen molecules and molecular ions, J. Phys. Chem. Ref. Data, 19, 3617–3636, 1990.

Vahedi, V. and Surendra, M.: A Monte Carlo collision model for the particle-in-cell method: applications to argon and oxygen discharges, Comput. Phys. Comm., 87, 179–198, 1995.

von Zahn, U., Hunten, D. M., and Lehmacher, G.: Helium in Jupiter's atmosphere: Results from the Galileo probe helium interferometer experiment, J. Geophys. Res., 103(E10), 22 815–22 830, 1998.

Waite Jr., J. H., Bagenal, F., Seward, F., Na, C., Gladstone, G. R., Cravens, T. E., Hurley, K. C., Clarke, J. T., Elsner, R., and Stern, S. A.: ROSAT observations of the jupiter aurora, J. Geophys. Res., 99(A8), 14 799–14 810, 1994.